Relaxation of electronic defects in pure and doped La_2O_3 observed by perturbed angular correlations

Doru Lupascu, Sönke Habenicht, Klaus-Peter Lieb, Matthias Neubauer, Michael Uhrmacher, and Thorsten Wenzel
II. Physikalisches Institut, Universität Göttingen, Bunsenstrasse 79, D37073 Göttingen, Germany
(Received 6 December 1995)

Slow recovery processes of the electronic environment following the electron-capture decay of ^{111}In can reduce the amplitude of the perturbed $\gamma\gamma$-angular correlation of a nuclear decay. This effect was used to quantitatively extract recovery rates of an electrically stable environment at the probe ion ^{111}Cd in La_2O_3. The recovery rates depend on the availability of electrons at the probe site, which in turn is governed by the concentration of electron sources and the transport mechanisms. Both properties are experimentally analyzed by variations of the temperature and oxygen partial pressure and by doping with two (Ba, Mg) and four-valent ions (Ce, Zr). Tunneling processes between defect levels in the band gap are proposed to account for the temperature dependence of the recovery rates. Unexpectedly, an enhanced electron availability is observed at temperatures below 200 K. The electric field gradients of substitutional ^{111}Cd and those generated by intrinsic defects and dopants are analyzed. A comparison to the probe ion ^{111m}Cd, not affected by electron capture, is presented. [S0163-1829(96)04025-8]

I. INTRODUCTION

Electrical conductivity in nonmetallic compounds is influenced by many different processes. In oxides, ionic conductivity dominates at elevated temperatures, while at low temperatures the conductivity is mostly governed by electronic charge carriers, whose concentration depends on the nonstoichiometry of the ionic lattice and the amount of foreign dopants. The propagation of the different charge carriers still is an open question for many compounds. Here, basically ionic diffusion, electron tunneling, and the excitation of electrons into the conduction-band-forming polarons can occur (the same applies to holes in the valence band). It is difficult to distinguish between these different transport mechanisms from conductivity measurements only.

Like Mössbauer spectroscopy, the perturbed $\gamma\gamma$-angular correlation method (PAC) is sensitive, through the hyperfine interaction, to the local electric and magnetic environment of a probe nucleus and thus also to localized charge carriers. PAC has long been applied to the investigation of stable defects in metals.[1] The mobility of ionic defects was then studied by PAC in semiconductors as well as insulators.[2,3] Only recently has the dynamics of electronic charge carriers been observed by PAC. In the case of Cr_2O_3, charge-state fluctuations of the chromium ions close to the PAC probe in thermal equilibrium were found.[4] A more complex distortion of the electronic configuration close to the PAC probe is generated by the electron-capture after effect (ECAE).[5–20] The Auger cascade following the EC decay leaves the probe ion in a highly ionized state.[21] If the recovery rate towards an undistorted stable electrical environment is fairly slow as compared with the reciprocal hyperfine frequency, the PAC signals are strongly modified. Recently, a method has been developed to correlate such recovery rates to the observed reduced amplitudes in PAC spectra.[22] Therefore, PAC is able to investigate the availability of electrons at the defect site formed by the probe ion itself.

The hexagonal modification of lanthanum oxide was chosen because it exhibits the strongest damping of the PAC spectra at room temperature (RT) among the oxides investigated so far. Furthermore, it contains only a single cation site with a symmetric electric field-gradient (EFG), ideal for PAC investigations. A well defined influence of the dopants is ensured as the chosen dopant oxides have a good miscibility with La_2O_3.

II. UNIDIRECTIONAL RELAXATION IN PERTURBED ANGULAR CORRELATIONS

In a PAC experiment the perturbation of the angular correlation of two consecutive nuclear γ rays is determined by the hyperfine interaction of the intermediate nuclear level with its electric environment (magnetic interactions are not considered here). The Fourier transform of a static PAC spectrum consists of a triplet of sharp frequencies (in the case of $I=5/2$ and $\eta\neq 1$) for each EFG acting on the probe nucleus (e.g., a particular crystallographic site). A damping of PAC time spectra occurs if different nuclei sense slightly different static EFG's due to distortions in their remote neighborhood. In a *dynamic* description, the environment of an individual nucleus changes during the lifetime of the sensitive level leading to dynamic damping and phase shifts in the spectra. Winkler and Gerdau developed a description of PAC spectra for dynamic hyperfine interactions based on stochastic processes:[23] The environment of a probe nucleus may instantaneously change between different environmental states. For a single site and a nuclear spin I the resulting perturbation factor $G_{22}(t)$ is then given in the most general form by

$$G_{22}(t)=\sum_{m_1=-I}^{I}\sum_{m_2=-I}^{I}\sum_{N=-N_{\max}}^{N_{\max}}(-1)^{2I+m_1+m_2}\times\begin{pmatrix} I & I & N_{\max}\\ m_1' & m_1 & N\end{pmatrix}\begin{pmatrix} I & I & N_{\max}\\ m_2' & m_2 & N\end{pmatrix}\times\sum_{a,b}p_a\left[bm_2m_2'\left|\left(-\frac{i}{\hbar}\mathcal{H}_{hf}^{\times}+\hat{R}\right)\right|am_1m_1'\right] \quad (1)$$

with

$$\left[bm_2m_2'\left|\left(-\frac{i}{\hbar}\mathcal{H}_{hf}^{\times}+\hat{R}\right)\right|am_1m_1'\right]=\sum_{k}^{a_{\text{tot}}^{*}36}(bm_2m_2'|T_k)\times(S_k|am_1m_1')e^{(-\lambda_k+i\omega_k)t}. \quad (2)$$

a and b denote different environmental states $\mathcal{H}_a^{\times}$, all acting on the identical nucleus (in the superHamiltonian $\mathcal{H}_{\text{hf}}^{\times}$ at positions $a=b$). p_a denotes the initial occupation of the environmental state a and a_{tot} is the total number of possible states. The relaxation matrix $\hat{R}$ contains the transition rates between the different environmental states. A detailed description how to handle superoperators for PAC is given in Ref. 23 and 22. Up to now, this theory has only been applied to fluctuating EFG's originating either from the diffusion of ions or vacancies,[23] the trapping and release of charges[2,4] or the cage motion of ions.[3] In all these cases the charge carriers were in thermal equilibrium with their environment.

The K-electron-capture of ^{111}In(EC)^{111}Cd when decaying to ^{111}Cd leaves the probe ion in a highly charged state far out of equilibrium. The inner electron orbitals are filled up from outer shells within about 10^{-14} s (Ref. 24) and thus much too fast to have any influence on the PAC spectra. At the same time, the probe ion loses quite a large number of electrons (3–8 on average, Ref. 21) due to Auger processes. Highly charged states of ions in a solid become compensated by electrons from their next-neighbor ions within less than about 10^{-12} s. Only ions with one or two extra charges (Cd^{3+} or Cd^{4+}) with respect to their appropriate charge state in the solid (Cd^{2+}) then may remain stable for times long enough to reach the sensitive time scale ($T_{1/2}$ = 85 ns) of the $I=5/2$ level in ^{111}Cd . In this ''time window of the measurement,'' transitions still occur to the stable Cd^{2+}, which in oxides is usually the stable electronic configuration of cadmium.

This physical situation was simulated with the program DYNXWW,[25] that was conceived to calculate any dynamic perturbation function based on Eq. (1).[22,26,27] Numerical solutions can be obtained for a set of initial states of arbitrarily chosen asymmetries and orientations in space and dynamic transitions between them. A stable final configuration is reached with a relaxation rate Γ_r and characterized by EFG_f. In this case of *unidirectional* relaxation, the spectra show the characteristic behavior of Fig. 1: All the phase shifts vanish if fluctuations between the initial states are allowed. We introduce the relative amplitude of EFG_f as $r=f_{\text{obs}}/f_{\max}$ where $f_{\max}$ denotes the maximum fraction found in static cases. r depends on the total relaxation rate Γ_r populating EFG_f. If experimentally more than one crystallographic site is occupied, the amplitudes r_i have to be considered for all fractions f_i of ions occupying different crystallographic sites i: $r_i=f_{\text{obs}}^i/f_i$ (Ref. 20).

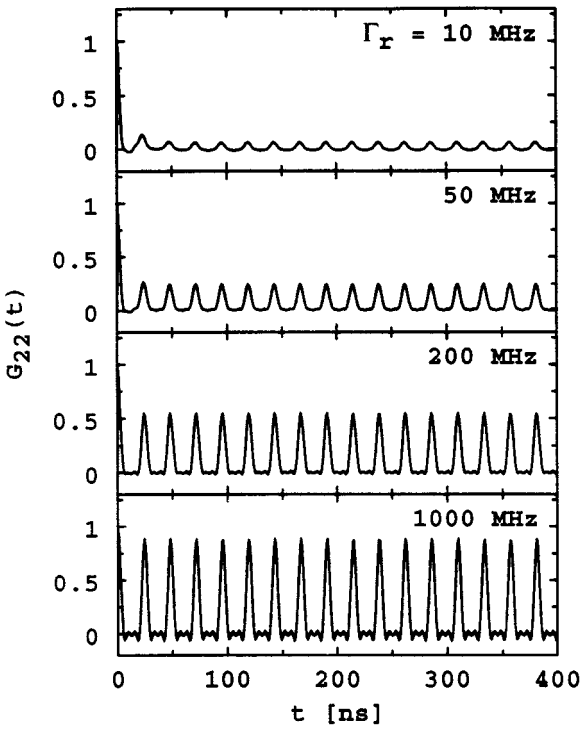

FIG. 1. Simulated spectra for ^{111}In in La_2O_3 for different recovery rates Γ_r after emission of the first γ ray. The displayed spectra were calculated for a transition rate between the initial EFG's of $\Gamma_i=20$ MHz.

Unidirectional relaxation for the particular case of the thermally activated breakup of defect ^{111}In pairs (EFG_i) into substitutional ^{111}In (EFG_f) in silicon or metallic zink has been discussed by Hoth and by Iwatschenko-Borho.[28,29] Two axially symmetric EFG's of identical orientation only differing in their coupling constants and distribution widths δ were considered. The perturbation factor is then given by

$$G_{22}(t)=\sum_n s_{2n}\{[1-a_n]\cos(n\omega_i t)e^{-(n\delta_i+\Gamma_r)t}-b_n\times\sin(n\omega_i t)e^{-(n\delta_i+\Gamma_r)t}+a_n\cos(n\omega_f t)e^{-n\delta_f t}+b_n\sin(n\omega_f t)e^{-n\delta_f t}\}, \quad (3)$$

$$a_n=\frac{\Gamma_r(n\Delta\delta+\Gamma_r)}{(\Gamma_r+n\Delta\delta)^2+(n\Delta\omega)^2},$$

$$b_n=\frac{\Gamma_r n\Delta\omega}{(\Gamma_r+n\Delta\delta)^2+(n\Delta\omega)^2},$$

$$\Delta\delta=\delta_i-\delta_f,\quad \Delta\omega=\omega_f-\omega_i. \quad (4)$$

It is important to note that the differences of the static distribution widths $\Delta\delta$, and of the coupling constants $\Delta\omega$, as well as the relaxation constant Γ_r, quadratically enter the amplitudes a_n and b_n. Furthermore, the final EFG_f is only

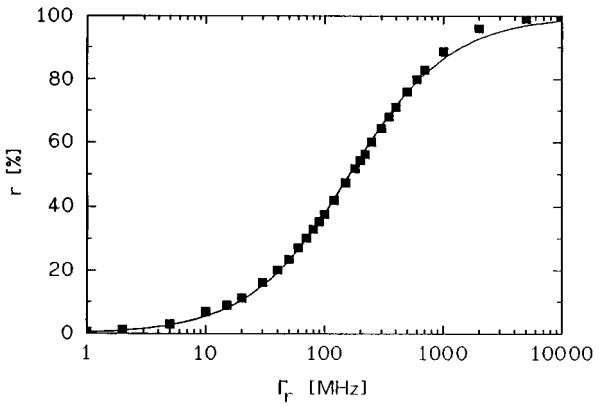

FIG. 2. Recovery rate-dependent amplitude r in a unidirectional relaxation model for La_2O_3. The continuous line is a fit of Eq. (3) to the calculated points.

damped by its own static distribution width δ_f, whereas EFG_i is also damped by the relaxation rate Γ_r. For large relaxation rates Γ_r the sine terms, i.e., the phase shifts, vanish. If EFG_f has a very narrow distribution width ($\delta_f \approx 0$), $\Delta\delta = \delta_i$ can be considered a measure of the distribution of the initial EFG_i.

The complete simulations of the unidirectional relaxation for substitutional ^{111}In in La_2O_3 in Fig. 1 showed that the spectra can be well approximated by Eq. (3) if r_1 is associated with $r_1 = a_1 = f_{\rm obs}/f$ for $f = 1$ (the slight difference of a_2 and a_3 as compared to a static fit are neglected here). The approximate values for $\Delta\delta$ and $\Delta\omega$ are determined by fitting

$$r_1 = \frac{\Gamma_r(\Delta\delta + \Gamma_r)}{(\Delta\omega)^2 + (\Delta\delta + \Gamma_r)^2} \tag{5}$$

to the amplitude r in Fig. 2.

III. EXPERIMENTAL PROCEDURE

Pressed powder samples of ultrapure La_2O_3 (Johnson and Matthey: La_2O_3 99.9999%, the content of any foreign ions was verified to be less than 0.05 at. %) were heated for 16 h at 1500 K in air to ensure purely hexagonal A-phase La_2O_3 as verified by x-ray diffraction. The samples were then cooled down to RT within 20 min. About 10^{12} $^{111}In^+$ ions were implanted at 400 keV into the samples by means of the Göttingen ion implanter IONAS.[30] The samples were annealed for 1 h at 1350 K in air to remove radiation damage. PAC measurements in the range from 20 to 290 K were carried out by means of a closed-cycle helium cryostate in a vacuum of 10^{-4} Pa. For PAC measurements above RT a vacuum oven reaching to about 1000 K was used and for higher temperatures (up to 1300 K) an oven in ambient air.[31] During all the preparation steps the samples were exposed to ambient air at RT for 20 min at maximum to avoid the takeup of air moisture.

The short-lived isotope ^{111m}Cd was implanted at an energy of 60 keV at the ISOLDE facility at CERN. The samples were then sealed in quartz tubes at about 2×10^4 Pa of air pressure ($\approx 10^5$ Pa at 1350 K) to avoid the diffusion of ^{111m}Cd out of the sample. Due to the short half life of the isomeric isotope ($T_{1/2} = 48$ min) the annealing time was reduced to 50 min.

In all the PAC setups, the maximum experimental $\gamma\gamma$ anisotropy was measured using a $^{111}InCl_3$ solution in distilled water enclosed in a plastic foil container, whose geometry was very similar to that of the samples. For the same purpose, ^{111m}Cd at ISOLDE was implanted into thin sodium chloride pellets, which were subsequently dissolved in distilled water.

To achieve a variation of the oxygen partial pressure, the vacuum chamber was flooded with dried oxygen. Then the oxygen flow into the chamber was gradually reduced by pumping to the desired pressure values ranging from 10^{-4} to 10^5 Pa.

La_2O_3 was doped with Ce, Zr, Mg, and Ca in different concentrations. The doped samples were prepared from $La(OH)_3$ that initially contained 0.18(5) at. % of Ba ions, which was confirmed by a separate inductively coupled plasma atomic emission spectroscopy measurement[32] (no other constituent exceeded 0.05 at. %). Quartz containers were cleaned with boiling nitride acid and then rinsed with doubly distilled water. The dopants [$Ce(IV)(OH)_4$, $Zr(IV)OCl_2$, $Mg(OH)_2$, and $CaCO_3$, all ''ultrapure''] were dissolved in concentrated nitride acid (metallic content < 0.07 ppm) and then mixed according to the metal content desired in the samples. The samples were dried under continuous stirring and then fully oxidized for 6 h at 1170 K. X-ray measurements confirmed the complete solubility of all dopants in the hexagonal La_2O_3 [up to 10 at. % (Refs. 33–35)].

IV. EXPERIMENTAL RESULTS

A. Temperature variation

Among all the influences on PAC spectra of ^{111}In-doped samples investigated in this work, the influence of temperature on pure La_2O_3 is the most important one. Figure 3 shows a set of spectra in La_2O_3 covering the temperature range from 12 to 823 K. All the spectra show one single EFG_1 of axial symmetry ($\eta_1 = 0$). Around RT the angular correlation disappears almost completely ($r_1 \approx 0$). Figure 4 shows the spectra observed with the probe ^{111m}Cd. The angular correlation in these spectra is practically independent of temperature and only the coupling constant ν_{Q1} changes (as in Fig. 3). The temperature dependence of the coupling constant ν_{Q1} for both probes is shown in Fig. 5. The EFG is exactly the same for both probe isotopes. Up to RT the EFG is constant: $\nu_{Q1} = 280.3(8)$ MHz, $\eta_1 = 0.005(5)$. Above RT the coupling constant linearly decreases with temperature according to

$$\nu_{Q1}(T_m) = 304(1)\ \text{MHz} - 0.069(1)\,\frac{\text{MHz}}{\text{K}}\,T_m\,. \tag{6}$$

This linear decrease is valid up to very high temperatures, even when the trapping of intrinsic defects occurs. Figure 6

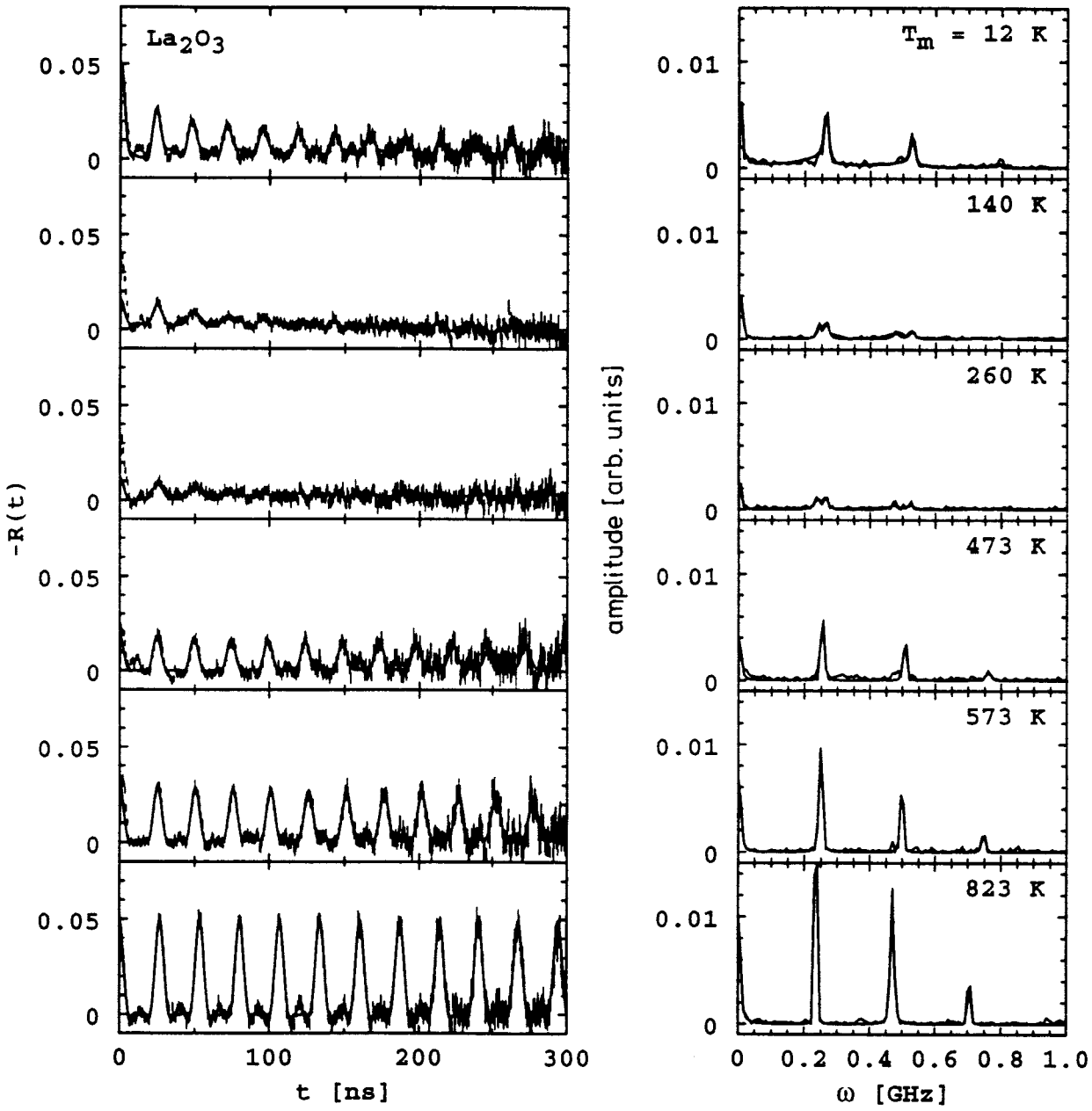

FIG. 3. Temperature-dependent spectra in La_2O_3 with ^{111}In.

displays the experimental amplitudes r_1 of EFG_1 for both probes at times longer than 10 ns. For ^{111}In this amplitude is strongly temperature dependent, having a deep minimum near RT, while it shows no temperature dependence for ^{111m}Cd. Around RT a second EFG is seen in very small amounts ($<3\%$), which has the same parameters as the Ce-induced EFG_2 (see below). It becomes visible only around RT, where the maximum damping for EFG_1 occurs.

B. Variation of oxygen pressure

The oxygen partial pressure was varied in order to check whether the concentration of holes, i.e., the main charge carriers in La_2O_3 at low temperatures, would alter the availability of electrons at the probe site or not. A reduction of the oxygen partial pressure reduces the number of La vacancies and due to charge neutrality three holes are annihilated along with each La vacancy. A first measurement consisted of a sample held at $T_m = 950$ K, the oxygen pressure varying from 10^{-4} to 10^{5} Pa. The measurements were performed with very high statistics, but *no* modification of the amplitude r_1 was found in the spectra. The measurement was then repeated at $T_m = 500$ K, where a stronger reduction of r_1 had been seen (see Fig. 6). To ensure that a change in the stoichiometry occurs, the samples were first annealed for 2 h at 950 K and the respective pressure, rapidly cooled down to 500 K and then measured under unchanged pressure conditions. Again *no* modification of the spectra with pressure was observed. A measurement at much lower p_{O_2} in a CO/CO_2-gas mixture and at higher temperatures partially drove the ^{111}In out of the sample and into metallic La.

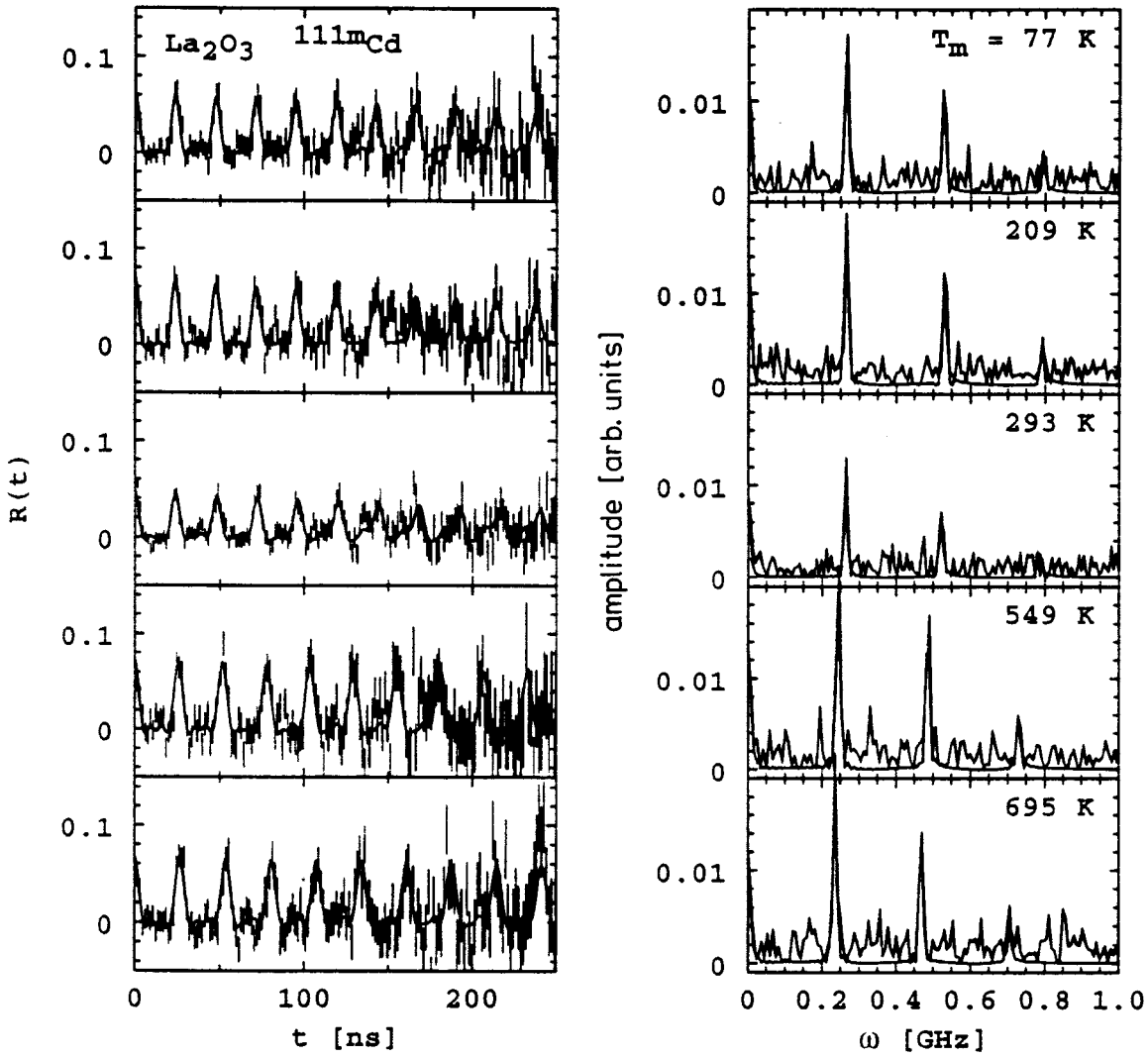

FIG. 4. Temperature-dependent spectra in La_2O_3 with ^{111m}Cd.

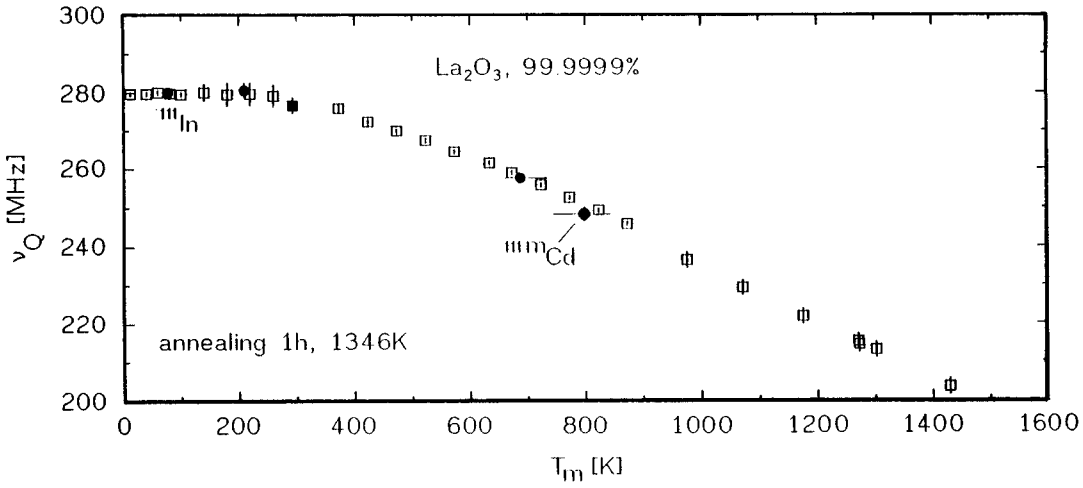

FIG. 5. Temperature dependence of ν_q with ^{111}In (open squares) and ^{111m}Cd (full dots). The asymmetry parameter is constantly $\eta \leqslant 0.005$.

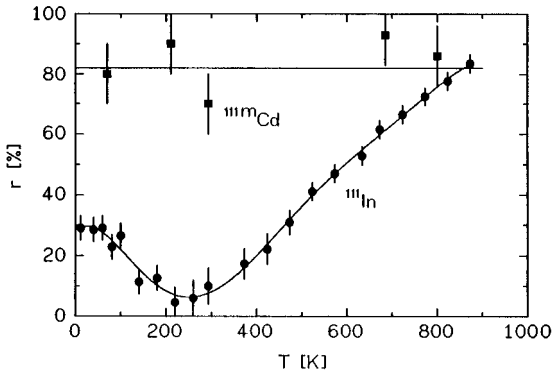

FIG. 6. Temperature dependence of the assigned amplitude r for a static fit with ^{111}In (squares) and ^{111m}Cd (full circles).

C. Intrinsic defects at high temperatures

At $T_m = 1176$ K in ambient air the trapping of defects at the probe ion was observed. Figure 7 shows the PAC spectra measured after different times. During the first 8 h only the undisturbed substitutional environment EFG_1 was seen [7(a)]. Then the substitutional fraction f_1 (at $T_m = 1176$ K $r_1 \approx 1$) gradually decreased and two new EFG's appeared, EFG_6 being asymmetric and EFG_7 symmetric [see Fig. 7(b) and Table I). After 56 h the fractions of EFG_6 and EFG_7 did not change any more, as can be seen in the inset of Fig. 7. In the RT spectrum (c) taken after quenching from 1176 K, the amplitude r_1 of EFG_1 for the remaining $f_1 = 30\%$ of substitutional ^{111}In ions vanished, while EFG_6 and EFG_7 were still well resolved. To test the binding of the trapped species to the probe ion, the sample was then measured at $T_m = 1270$ K and the defects remained at the probe. After a new annealing for 2 h at 1430 K, removing all the neighboring defects, at $T_m = 976$ K again only EFG_1 with $f_1 = 100\%$ was observed [Fig. 7(d)]. The last spectrum of this series taken at RT again showed the complete reduction of the amplitude $r_1 \approx 0$ for the substitutional ^{111}In ions in La_2O_3.

TABLE I. Hyperfine parameters and capture rates for intrinsic defects at $T_m = 1176$ K.

	ν_Q (MHz)	η	δ (MHz)	τ_E (h)	f (%)	t_0 (h)
EFG_1	222(1)	0.00(1)	0.4(3)	9(2)	26(3)	0
EFG_6	78(4)	0.9(1)	6(2)	18(16)	21(6)	8(4)
EFG_7	100(4)	0.0(1)	5(2)	10(10)	19(6)	21(2)

D. Doped samples

Doping is another means to alter the concentration of charge carriers. A first set of PAC measurements was performed in La_2O_3 predoped with 0.18(5) at. % Ba, and additional doping with Ce ions. This initially unintentional Ba counter doping had the advantage of fully ionizing the dopant ions (see, e.g., Ref. 36). Figure 8 shows three sets of temperature-dependent Fourier spectra without any Ce and with 0.1 and 0.35 at. % Ce. Several new EFG's became observable. At Ce concentrations $\geqslant 0.35$ at. % and elevated temperatures only the substitutional EFG_1 was visible. Around RT a second EFG_2 with a slightly lower coupling

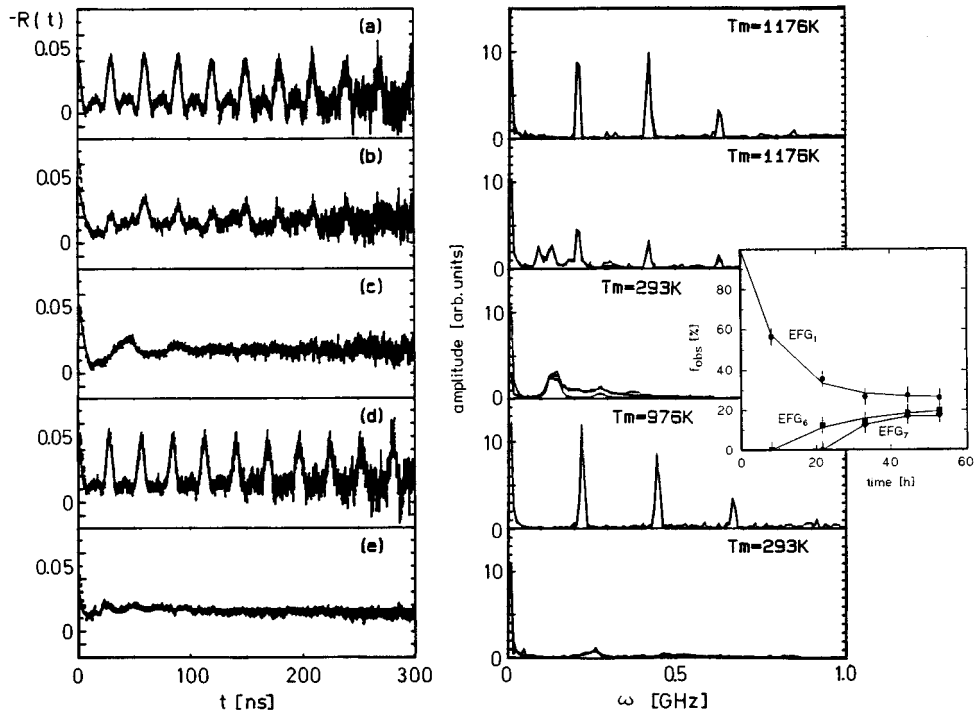

FIG. 7. Trapping of defects at ^{111}In in La_2O_3: (a) PAC spectrum at 1176 K after 8 h, (b) at 1176 K after 56 h, (c) subsequent room temperature spectrum, (d) spectrum at 976 K, after 2h10' annealing at 1430 K, (e) subsequent room-temperature spectrum. Insert: Time dependence of trapping of impurities at the undersized ^{111}In-ion in La_2O_3 at $T_m = 1177$ K in air. At times longer than 45 h no further impurities are trapped at ^{111}In. The continuous lines are fits to the data with $f_{sub}(t) = f_{fin} + (1 - f_{fin})\exp(-t/\tau_{E_{sub}})$ for the reduction of the substitutional fraction and $f_{1,2}(t) = f\exp[-(t-t_0)/\tau_E)]$ for the increase of fraction of the observed defects.

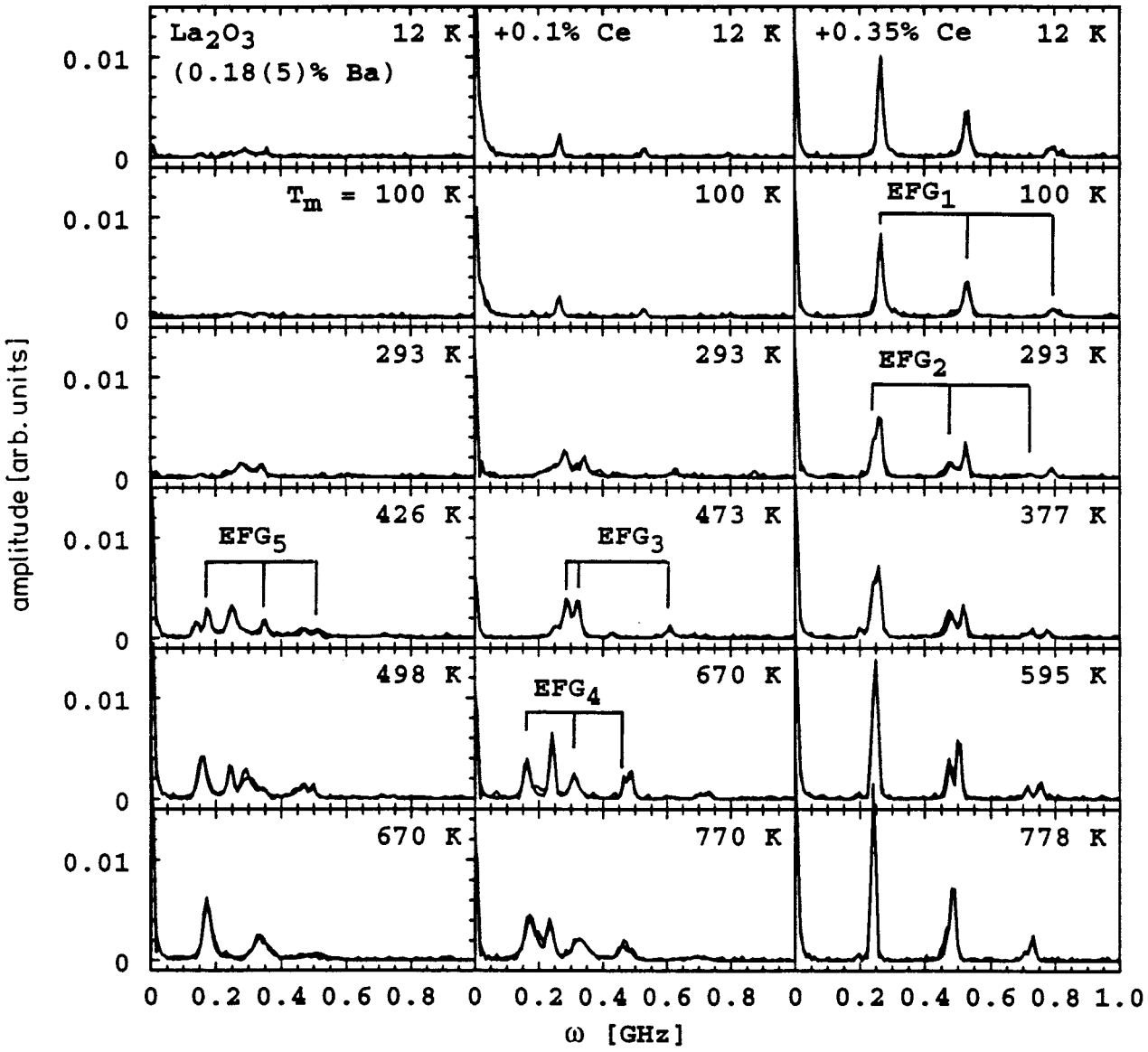

FIG. 8. Temperature-dependent PAC spectra observed with (left) Ba dopants, (center) additional doping of Ce to about compensating conditions, and (right) strong Ce doping.

constant was observed in the 0.35 at. % Ce-doped sample, vanishing below 200 K. Figures 9(a) and 9(b) show the temperature dependence of ν_{Q2} and f_2 as compared to ν_{Q1} and f_1 in this sample. Figure 9(b) clearly shows that for the 0.35 at. % Ce-doped sample the observed fraction $f^1_{\rm obs}$ for EFG_1 is higher than for pure La_2O_3: Although the appearance of EFG_2 aggravates the observation of the relaxation phenomena, the r_1 value after Ce doping is found to be higher in the minimum region around 260 K. To avoid possible errors in the r_1 estimation the sum of both EFG's is considered for presentation in Figs. 9(b) and 10(c), for which the increase of the observable fraction is found to be enhanced and can be measured very clearly. For higher Ce concentrations of 0.5–5 at. % Ce, the fraction of EFG_2 was again reduced but was still discernable for 1 at. % Ce and EFG_1 was broadened.

A doping of La_2O_3 with 1 at. % Zr did not result in the observation of EFG_2. The amplitude r_1 behaved similarly as r_1 in the sample with 5 at. % Ce. Figure 9(c) shows the temperature dependence of fraction f_1 observed in the Zr-doped sample, which is also compared to samples with 0.35, 1, and 5 at. % Ce.

Three EFG's (EFG_3, EFG_4, and EFG_5) arose when the samples were doped with Ba ions [Fig. 8(a)]. They were also observed in Ce-doped samples with lower Ce concentrations than the unintentional 0.18 at. % Ba concentration. Their EFG parameters and the temperature range of their appearance are given in Table II. Only EFG_3 was strongly temperature dependent. At RT and below, the PAC spectra of all the samples without any additional Ce doping were completely damped ($r_3, r_4, r_5 \approx 0$). Around RT, EFG_3 was dominant in the spectra, but at higher temperatures it was partially replaced by EFG_4. Further doping with the two-valent ions (Mg,Ca) did not modify the spectra as compared to the sample with 0.18(5) at. % Ba. Figures 10(a) and 10(b) show the temperature dependence of $f_{\rm obs}$ for EFG_3 and EFG_4.

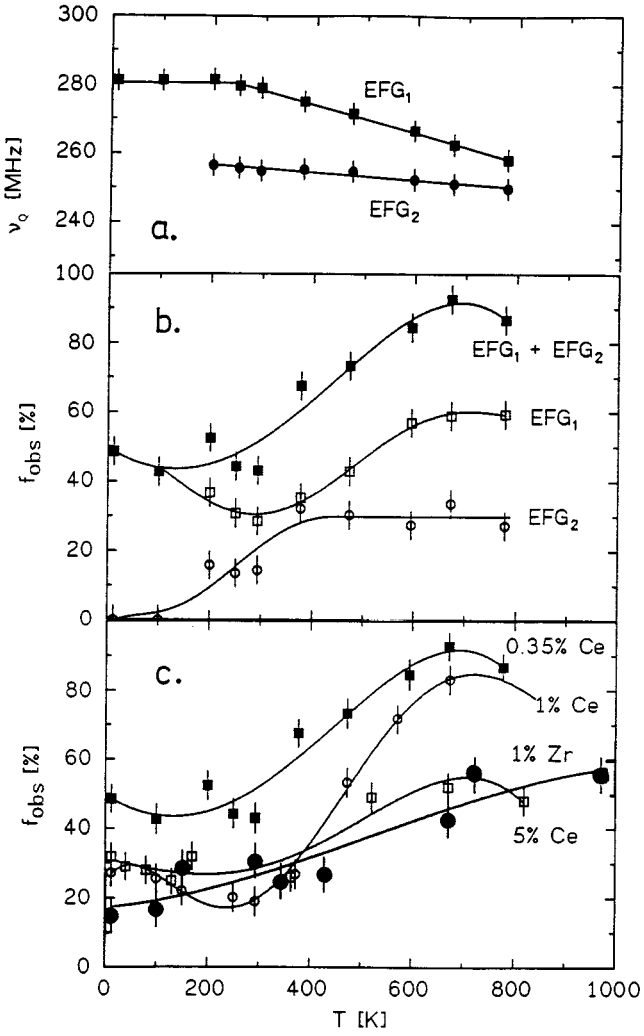

FIG. 9. (a) Temperature dependence of the coupling constants of EFG_1 and EFG_2 observed with cerium dopants. Both EFG's have $\eta<0.1$. (b) Fraction of both EFG's in a sample containing 0.35 at. % Ce. (c) Fraction of EFG_1 in a Zr-doped sample (1 at. %) compared to 1 at. % Ce and 5 at. % Ce-doping.

As all the samples had a base concentration of 0.18 at. % Ba, the additional doping with similar amounts of Ce ions resulted in a compensation of the dopants. At such intermediate Ce concentrations of about 0.1 at. %, EFG_1 appeared at temperatures well above and well below RT (see Fig. 8), but not at RT itself—a behavior similar to the one in ultrapure La_2O_3. With rising Ce content, EFG_3 and EFG_4 were replaced by EFG_1 and EFG_2. At the same time the total assignable amplitude $\Sigma f^i_{\rm obs}$ was raised to a maximum value at 0.35 at. % Ce concentration and then dropped back down with rising Ce content [Fig. 10(c)]. EFG_5 only appeared near RT in samples quenched from above 700 K. While EFG_3 and EFG_4 have somewhat larger distribution widths, the frequency triplet of EFG_5 is very sharp (see Table II).

V. DISCUSSION

A. The after effect, a unidirectional relaxation process

The central question in the discussion will be the understanding of the temperature-dependent damping in the spectra of ultrapure La_2O_3 (Fig. 3) with the minimum amplitude

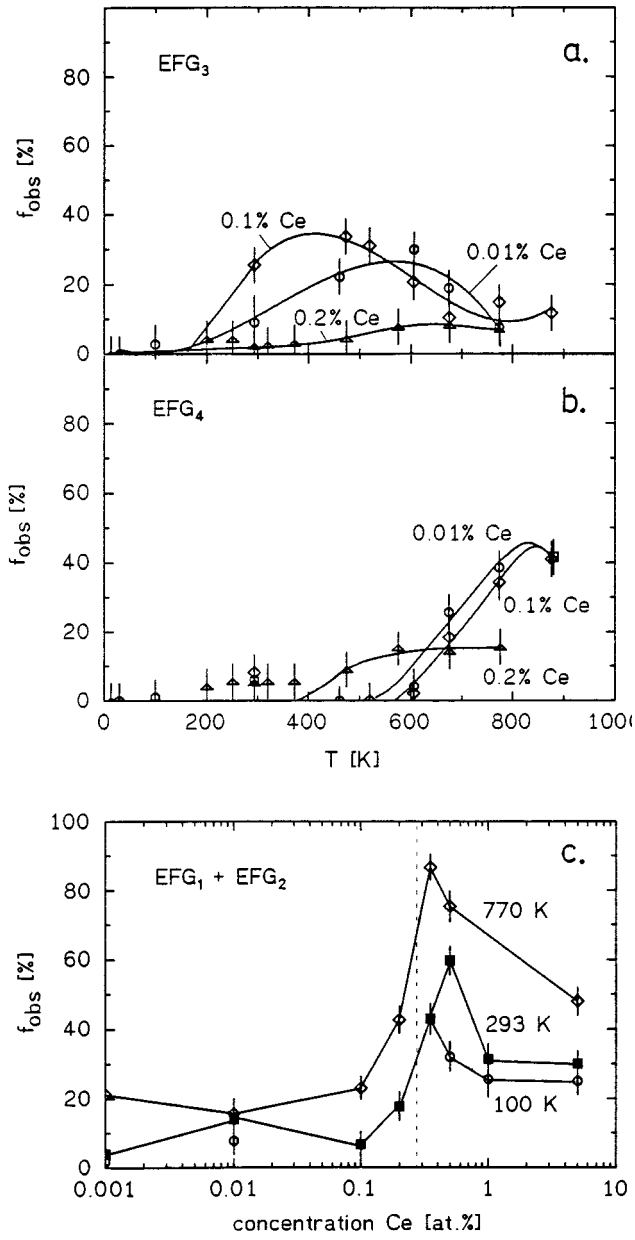

FIG. 10. Fractions of (a) EFG_3, (b) EFG_4, and (c) the sum of EFG_1 and EFG_2 for different Ce concentrations.

TABLE II. Hyperfine parameters of the EFG's in doped samples at the temperatures indicated. The range of occurance of each EFG is given. ω_1 and ω_2 are also included for better recognition in the experimental spectra.

	Temperature range [K]	T_m [K]	ν_Q [MHz]	η	δ [MHz]	ω_1 [MHz]	ω_2 [MHz]
EFG_1	12–900	293	279(1)	0.01(1)	2(2)	263(1)	526(2)
EFG_2	12–900	293	255(1)	0.02(2)	2(2)	240(1)	481(2)
EFG_3	12–600	293	198(3)	0.78(1)	8(4)	283(4)	341(5)
EFG_4	400–900	673	166(5)	0.16(1)	8(4)	161(5)	311(9)
EFG_5	(200–490)	426	185(5)	0.02(2)	4(3)	174(5)	350(9)

around $T_m = 250$ K (Fig. 6). As already described in Sec. II, the electron-capture decay of ^{111}In produces a highly unstable physical situation. As a consequence of the EC decay, at least one electron is missing to transform the probe into the stable $^{111}Cd^{2+}$ ion. We propose that a delayed electron supply to the probe due to the electronic structure of La_2O_3 causes the damping of the PAC spectra. The most direct proof of this assumption is the PAC measurement with ^{111m}Cd which is not affected by a chemical transmutation: Without a preceding electron capture the spectra are undamped (Figs. 4 and 6).

The second strong hint is the characteristic, temperature dependence of the reduced amplitude r_1 of the ^{111}In spectra themselves (300 to 900 K, Fig. 3). At times longer than 10 ns no further damping of the perturbation functions $R(t)$ was observed and the amplitude of the oscillations stays constant—exactly the same behavior was found in the simulations of a unidirectional relaxation described above.

The temperature dependence of the coupling constant ν_{Q1} is a third indicator of a unidirectional relaxation. Below RT, ν_{Q1} is constant, but steadily drops for higher temperatures. Comparing this to results obtained previously in Cr_2O_3,[4] at first sight a fluctuation regime between two EFG's might be assumed. In a fluctuation regime, however, the second stable EFG should occur at a higher temperature, where it stays constant. An exponential damping would also be seen at the intermediate temperatures, where the transition in ν_Q occurs. As ν_{Q1} in La_2O_3 drops linearly up to very high temperatures and does not stabilize at a certain value, as furthermore, no exponential damping is observed and, finally, precisely the same temperature dependence was observed with ^{111m}Cd probes, a fluctuation regime can definitely be excluded.

The amount of electrons available in a solid can be altered by temperature. Additional intrinsic sources of electrons (or holes) in a nonstoichiometric oxide are vacancies (V_O for $e-$, V_{La} for h^+). In the rare-earth sesquioxides (R_2O_3) a conversion from p conductivity for high oxygen pressure to n conductivity at low p_{O_2} occurs between $p_{O_2} = 100$ and 1 Pa,[37–40] depending on the particular oxide and the temperature. However, neither the hexagonal A phase of Nd_2O_3 (Ref. 39) nor the one of La_2O_3 (Refs. 37 and 40) shows n conductivity; at least its contribution was not well resolved in the conductivity measurements. This fact is confirmed by the PAC results: A strong lowering of p_{O_2} did not lead to n conductivity in hexagonal La_2O_3. Furthermore, the transport mechanism to the ^{111}Cd defect level seems to neither depend on the concentration of holes in the valence band nor on the concentration of La or O vacancies.

A definite means to introduce donor (or acceptor) states is the doping with foreign ions. To increase the concentration of free electrons the samples were doped with the four-valent ions Ce and Zr. The spectra were significantly less damped around RT than in pure La_2O_3. The minimum damping was achieved for a concentration of Ce that yields fully ionized Ce^{4+} ions as can be seen from the dependence of the total observed amplitude $\Sigma_{i=1}^{2} f_{\text{obs}}^{i}$ on the Ce concentration (Fig. 10). Zr proved to be somewhat less effective. The full amplitude $r_1 = 1$ was obtained with none of the two dopants at RT, though. Purely two-valent doping, on the other hand, fully reduced the amplitude to $r_1 = 0$ at temperatures below RT. Thus, the Ba ions in the bulk trap the few electrons originally available at the probe site at low temperatures. Only at higher temperatures was a finite amplitude r_1 seen in the spectra.

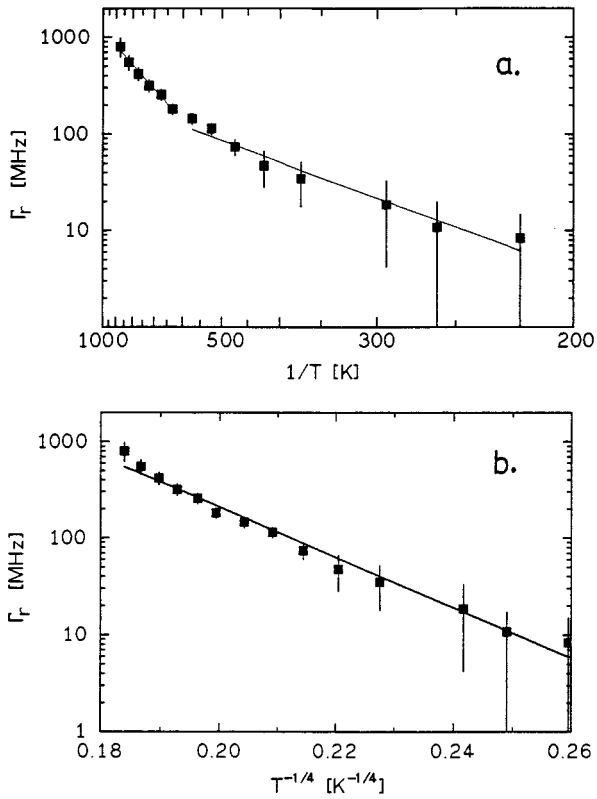

FIG. 11. Temperature dependence of the relaxation rate of an unperturbed environment of ^{111}In in La_2O_3 for temperatures above 260 K: (a) in an Arrhenius plot and (b) for variable-range hopping $1/T^{1/4}$-dependence.

All these PAC results prove that the ECAE has to be described as a *unidirectional relaxation* regime and that an *electron* transport process determines the reduced amplitude r_1 and the relaxation rate Γ_r in the spectra. Therefore, the approach of Sec. II was applied to the PAC data to draw conclusions on the relaxation rate Γ_r. The calculated dependence of the reduced amplitude r_1 on Γ_r in the particular case of La_2O_3 ($\nu_{Q1} = 280$ MHz, $\eta_1 = 0$) is plotted in Fig. 2. The two parameters $\Delta\delta = 156(5)$ MHz and $\Delta\omega = 47(16)$ MHz were determined according to Eq. (3).

B. Electron transport mechanism

In a wide band-gap semiconductor like La_2O_3, electrons can be furnished (i) from the conduction band due to thermally excited electrons of defect levels energetically close to the conduction band, (ii) from the valence band forming a hole, (iii) from a nearby defect level (e.g., a next-neighbor impurity) or, (iv) finally by hopping of electrons between defect levels (variable-range hopping). To decide on the nature of the electron-transport mechanism, which governs the present ECAE experiments, a comparison of conductivity measurements and PAC results is helpful. Figure 11(a) shows the Arrhenius plot of the deduced transition rates.

Two separate processes can be distinguished with a transition at approximately 600 K and the activation energies $E_{>600\ \mathrm{K}}=0.28(10)$ eV and $E_{<600\ \mathrm{K}}=0.1(1)$ eV. Conductivity measurements show a similar transition temperature $T_{\mathrm{cond}}=540$ K, but the activation energies are drastically higher $E_{>540\ \mathrm{K}}=1.05$ eV and $E_{<540\ \mathrm{K}}=0.7$ eV.[38] Consequently, one has to conclude that a different process underlies the thermal excitation observed here: The dominant *p*-type conductivity of La_2O_3 does not play the major role in the availability of electrons at ^{111}Cd, despite the similar transition temperature. Therefore, we have to believe that thermally excited electrons in the conduction band are the origin of the observed temperature dependence. They have to originate from defects that neither take part in the conductivity process nor are annihilated rapidly by the dominant holes, i.e., they have to be located in the proximity of the probe ion.

The only band known from x-ray photoemission spectroscopy of La_2O_3 close to the Fermi energy is the O_{2p} band with a band gap of 2.4(1) eV.[41,42] Even though the band gaps determined by other authors differ largely, there is common agreement that above 500 K the principal conductivity contribution results from *p*-type hole conduction and, furthermore, that the band gap exceeds 2.3 eV. The very short lifetime (few fs) of holes in the valence band (O_{2p}) of La_2O_3 indicates that the short-range mobility of holes is very high. Nevertheless, the charge-carrier concentration is low due to the very small deviation from ideal stoichiometry.[43,39] Thus a scenario with two activation energies would have to originate from two different valence bands separated by only 0.2 eV. A direct thermal activation of charge carriers to ^{111}Cd, if possible at all, cannot originate from the valence band.

The picture of variable-range hopping (VRH) assumes charge carriers which tunnel between defect levels of similar energy in the band gap. A good test for this model is the characteristic $T^{-1/4}$ dependence of the mean hopping probability.[47] VRH has been reported from conductivity measurements in other chalcogenides, especially for In_2O_3 (Refs. 44 and 45) and $CdIn_2S_4$.[46] In our context, the bixbyite oxide In_2O_3, which shows very similar PAC data compared to the present ones in La_2O_3,[20] is of considerable interest. As this oxide is a dominating *n*-type conductor we can expect conductivity measurements as well as PAC experiments in this substance to directly test the electron-transport mechanism. La_2O_3, on the other hand, is a dominant *p* conductor. PAC results in this case may be independent of the majority holes. In fact, the best fit to the experimental relaxation rates in La_2O_3, shown in Fig. 11(b), yields the characteristic $T^{-1/4}$ temperature dependence, typical for VRH, which is also found for the relaxation rates with PAC in In_2O_3.[20]

Below $T_m=260$ K the amplitude of the PAC spectra rises again to about $r_1 = 0.3$ at 80 K and remains constant for lower temperatures. The higher availability of electrons at low temperatures may be due to a transition from insulating to metallic behavior of the host material, or to an enhanced tunneling probability. In the case of metallic conduction large amounts of electrons would reach the probe site and the full anisotropy ($r_1=1$) should be attained again at low temperatures. As this is not observed in the experiments, an enhanced tunneling probability seems to be more reasonable. Figure 12 shows the low-temperature part of the relaxation rate of EFG_1. In the picture of VRH the average tunneling distance between defect levels is proportional to $(T_0/T)^{1/4}$ and has to rise with decreasing temperature.[48] This leads to an increase of the average number of defects which can ''emit'' an electron to the Cd site and one expects approximately $\Gamma_r \propto T^{-3/4}$. The continuous line in Fig. 12 is a fit of such a temperature dependence to the experimental points above $T_m=$ 60 K. Unfortunately, the number of the responsible defects is not known for these samples. Consequently, an estimation of the average tunneling distance is not possible.

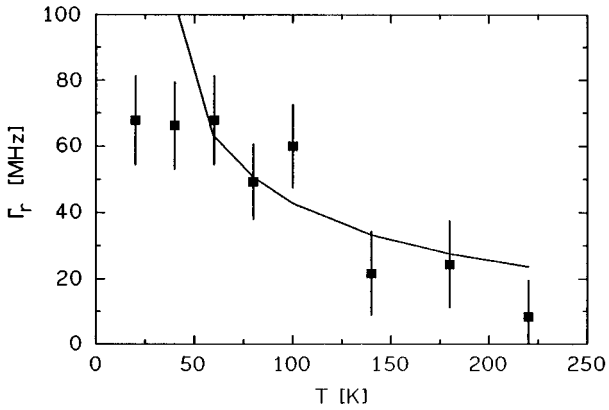

FIG. 12. Relaxation rates below 260 K. The continuous curve is a fit of $\Gamma_r \propto T^{-3/4}$.

The transition from the high- to the low-temperature regime in the PAC data for La_2O_3 at about 260 K is consistent with the freeze-in of phonons in La_2O_3 found in heat-capacity measurements.[49] At high temperatures a phonon-assisted long-range transport yields the high-temperature VRH. At intermediate temperatures the long-range transport ceases, but the individual hopping distance to the probe site is still too small to carry an effective charge transport. Later this becomes possible at even lower temperatures.

C. The strength of EFG_1

For most oxides investigated with ^{111}Cd so far, the point-charge model (PCM) is valid once the ionic distances exceed $d_{\mathrm{Cd\text{-}O}} \geqslant 210$ pm.[50,51] In these calculations the charges of the environing ions are located at the crystallographic sites producing the lattice EFG. Due to the probe's atomic shell, this value is enhanced by the Sternheimer antishielding factor $1-\gamma_\infty=32.95$,[52] which is calculated for an isolated Cd^{2+} ion to reproduce the EFG at the site of the probe nucleus. In the present case of La_2O_3, the PCM fails, although all interionic distances are large ($d_{\mathrm{La\text{-}La}}=385$ pm, $d_{\mathrm{La\text{-}La'}}=385$ pm, $d_{\mathrm{La\text{-}O_1}}=237$ pm, $d_{\mathrm{La\text{-}O_1'}}=246$ pm, $d_{\mathrm{La\text{-}O_2}}=273$ pm). For substitutional ^{111}Cd in La_2O_3 the calculated value for the coupling constant is $\nu_Q=$ 70 MHz compared to the experimental value of $\nu_Q=$ 279 MHz. Introducing lattice distortions is not enough, as—irrespective of the position along the *c* axis—the calculated value never exceeds 100 MHz. Only if the probe approached the next-neighbor oxygen ion overly close, or if it occupied an interstitial position, the experimental EFG could be reproduced by the PCM. One might speculate on the influence of covalent bonding, which could, de-

TABLE III. Ionic radii of dopants compared to La^{3+} (Ref. 56) (ordered for increasing mass).

Element	Formal charge	Ionic radius (pm)
Mg	+2	66
Zr	+4	79
Cd	+2	97
In	+3	81
Ba	+2	134
La	+3	101.6
Ce	+3	103.4
	+4	92

spite the long interatomic distances, drastically alter the charge distribution around the probe.

The linear drop of ν_{Q1} above RT (Fig. 5) can qualitatively be explained by the thermal-expansion of the lattice. Unfortunately, thermal-expansion data below RT are not known. An anisotropic expansion could explain that ν_{Q1} stays constant below RT. A stabilization of covalent bonds between the La ions below RT might be responsible for the constant value of ν_{Q1} at low temperatures. Such a covalent stabilization of the La planes in the hexagonal lattice was previously proposed to interpret the neutron-diffraction structure data in La_2O_3.[53,54] It can be taken as an independent additional hint to the influence of covalency in La_2O_3.

D. Structure of the defect-induced EFG's

Besides the already discussed modification of the concentration of free charge carriers, additional information can be obtained from the PAC results for the doped samples. We explain the newly appearing EFG's by the formation of ^{111}In-impurity/defect pairs during the annealing as they are usually observed in semiconductors.[55] The Ce ion exists in the two charge states Ce^{4+} and Ce^{3+}, which are dominant at different temperatures. We propose that Ce^{4+} and, similarly, Zr^{4+} are located not too far away from the ^{111}In probe, where they act as donors. This results in a less damped substitutional EFG_1. In the case of equally charged ions the ionic radius will play the most important role: Ce^{3+} is slightly larger than La^{3+} (see Table III), so it may form a pair with the distinctly smaller In^{3+} during the annealing. This pair is characterized by the slightly different EFG_2 due to lattice distortions. The much smaller Zr^{4+}, on the other hand, does not form any pairs with In^{3+} and thus only EFG_1 is observed.

After doping with Ba ions, three new EFG's are observed. Pair formation between ^{111}In and Ba is even more likely than for Ce ions. We propose that trapping of a Ba ion next to the probe causes EFG_3 and EFG_4. As both EFG's reversibly appear with temperature they have to be thermally stable configurations. It cannot be unambiguously decided whether the transition from EFG_3 to EFG_4 is generated by additionally stabilized oxygen vacancies or by different charge states of the defect pair. The amplitudes f_{obs} of EFG_3 and EFG_4 never add up to 100% in both configurations. Therefore, some dynamic damping has to be present at all temperatures, although a precise determination of this dynamics is not possible since linebroadening effects and distributions cannot be clearly excluded. EFG_5 was only seen at RT in quenched-samples. As the doping with Ba ions stabilizes oxygen vacancies, we propose EFG_5 to be a quenched next-neighbor oxygen vacancy, which is not thermally stable in the proximity of the probe ion at low temperatures but becomes observable in a quenched sample.

A further doping with other two-valent ions (Mg or Ca) did practically not alter the spectra as compared to only 0.18(5) at. % Ba doping in the whole temperature range. Thus all In ions are still trapped at the Ba ions and the further addition of holes to the valence band does not modify the availability of electrons at the probe. Now we can look back into the compensation region where the concentrations of Ba and Ce are similar. Due to the rising Ce concentration, finally all Ba ions are bound to Ce ions and the probe ion ^{111}In can trap the excessive Ce ions forming the Ce-In pairs clearly visible in the whole temperature range.

The defects trapped in the high-temperature measurement in ultrapure La_2O_3 definitely do not belong to any of the additional dopant ions used in the doping experiments. Even though oxygen vacancies are a minority species, they may be the trapped species. Some very small numbers of other dopants cannot be excluded either. The stable ^{111}Cd isotope implanted along with ^{111}In is a possible candidate, but to prove the nature of this trapped defect, separate measurements are needed.

VI. SUMMARY

The scope of this work was to study electronic arrangement processes following the ^{111}In(EC)^{111}Cd radioactive decay in La_2O_3. The isotope ^{111}In formed the source for the highly ionized defect through the electron-capture radioactive decay, and at the same time was used as the nuclear probe ^{111}Cd in the PAC measurements. While the PAC observation was sensitive to the total availability of electrons at the probe, external parameters were used to disentangle the influences of charge-carrier concentration and transport processes.

The temperature-dependent spectra showed that around room temperature very slow processes dominate the electron availability at the probe ($\Gamma_r \simeq$ 20 MHz). Basically, two electron-transport processes were shown to be possible in La_2O_3, the first one through the conduction band and the second one by VRH between interacting defect levels. A definite distinction between these two transport mechanisms was not possible, but in the case of conduction-band transport severe restrictions had to be imposed on the type of electron sources. By varying the oxygen pressure it was shown that the availability of electrons at the probe site is independent of the amount of holes in the valence band, the majority carrier in La_2O_3. Thus the variable-range-hopping conduction is favored by the authors. At low temperatures a direct local transport from defect levels was proposed to account for the enhanced availability of electrons.

The doping of La_2O_3 with Ce and Ba yielded two essential results: The amount of free charge carriers could be enhanced by four-valent doping. While the recovery rate of stable electric environments of the probe was less than 20 MHz in pure La_2O_3 at RT and in Ba-doped samples at RT and below, fully ionized Ce^{4+} ions raised the availability of electrons at the probe site by at least one order of magnitude in the whole temperature range and especially at RT ($\Gamma_r \simeq$ 200 MHz). Furthermore, size-attracted pairs of Ce-(^{111}In)

and Ba-(^{111}In) were formed during the annealing process after implantation of the ^{111}In probes, yielding distinctly different EFG's.

ACKNOWLEDGMENTS

The authors would like to thank L. Ziegeler for his help with the preparation of the doped samples. We thank the ISOLDE collaboration for the ^{111m}Cd implantations. We very much thank the Erlangen PAC group for their great help during the ISOLDE beamtime and D. Wieshow and H. Ruppert for determining the impurity concentrations in the doped and undoped samples. Furthermore, we would like to thank A.F. Pasquevich and J. Gardner for fruitful discussions on dynamic interactions and the ECAE. This work was supported by the Deutsche Forschungsgemeinschaft (Li325/2).

[1] F. Pleiter and C. Hohenemser, Phys. Rev. B **25**, 106 (1982); in *Hyperfine Interaction of Radioactive Nuclei*, edited by J. Christiansen (Springer, Berlin, 1983).
[2] N. Achtziger and W. Witthuhn, Phys. Rev. B **47**, 6990 (1993).
[3] R. Wang, J.A. Gardner, W.E. Evenson, and J.A. Sommers, Phys. Rev. B **47**, 638 (1993).
[4] M. Neubauer, A. Bartos, K.P. Lieb, D. Lupascu, M. Uhrmacher, and T. Wenzel, Europhys. Lett. **29**, 175 (1995).
[5] M. Deicher, Hyperfine Interact. **79**, 681 (1993).
[6] P. Lehmann and J. Müller, J. Phys. Radium **17**, 526 (1956).
[7] M. Salomon, L. Boström, T. Lindqvist, M. Perez, and M. Zwanziger, Ark. Fys. **27**, 97 (1964).
[8] H. Frauenfelder and R.M. Steffen, in *Alpha-, Beta-, Gamma-Ray Spectroscopy*, edited by K. Siegbahn (North-Holland, Amsterdam, 1965).
[9] U. Bäverstam, R. Othaz, N. de Sousa, and B. Ringström, Nucl. Phys. A **186**, 500 (1972).
[10] H. Barfuss, G. Boehnlein, H. Hohenstein, W. Kreische, M. Meinhold, H. Niedrig, and K. Reuter, J. Mol. Struc. **58**, 147 (1980).
[11] A.G. Bibiloni, J. Desimoni, C.P. Massolo, Mendoza-Zélis, A.F. Pasquevich, F.H. Sánchez, and A.R. López-García, Phys. Rev. B **29**, 1109 (1984).
[12] P.W. Martin, S.R. Dong, and J.G. Hooley, J. Chem. Phys. **80**, 1677 (1984); P.W. Martin, S.R. Dong, and J.G. Hooley, Chem. Phys. Lett. **105**, 343 (1984).
[13] H. Wolf, S. Deubler, D. Forkel, H. Foettinger, M. Iwatschenko-Borho, F. Meyer, M. Renn, and W. Witthuhn, Mater. Sci. For. **10-12**, 863 (1986).
[14] W. Bolse, M. Uhrmacher, and K.P. Lieb, Phys. Rev. B **36**, 1818 (1987).
[15] A.G. Bibiloni, J. Desimoni, C.P. Massolo, and M. Renteria, Phys. Rev. B **38**, 20 (1988).
[16] H. Jäger, H.T. Su, J. Gardner, I-Wei Chen, J.C. Haygarth, J.A. Sommers, and R.L. Rasera, Hyperfine. Interact. **60**, 615 (1990).
[17] A. Bartos, Ph.D. thesis, University of Göttingen, 1991.
[18] A. Bartos, K.P. Lieb, A.F. Pasquevich, M. Uhrmacher, and ISOLDE Collaboration, Phys. Lett. A **157**, 513 (1991).
[19] S. Habenicht, D. Lupascu, M. Neubauer, M. Uhrmacher, L. Ziegeler, and K.P. Lieb, Hyperfine Interact. C **1**, 250 (1996).
[20] S. Habenicht, D. Lupascu, M. Uhrmacher, L. Ziegeler, and K.P. Lieb, Z. Phys. B (to be published).
[21] T.A. Carlson, W.E. Hunt, and M.O. Krause, Phys. Rev. **151**, 41 (1966).
[22] D. Lupascu, Ph.D thesis, Universität Göttingen, Cuvillier, Göttingen, 1995.
[23] H. Winkler and E. Gerdau, Z. Phys. **262**, 363 (1973); H. Winkler, Z. Phys. A **276**, 225 (1976).
[24] O. Keski-Rahkonen and M.O. Krause, Atomic Data Nucl. Data Tables **14**, 139 (1974).
[25] D. Lupascu, program DYNXWW, program for calculating perturbation functions of fluctuating EFG's between arbitrary coordinate systems, contains the NAG© routines F01AMF, F01AVF, F01AWF, F02ARF, F04ADF, the code was cross checked with analytical solutions from Ref. 28.
[26] D. Lupascu, M. Neubauer, S. Habenicht, T. Wenzel, M. Uhrmacher, and K.P. Lieb, in *Condensed Matter Studies by Nuclear Methods*, edited by K. Tomala and E. A. Görlich (Institute of Physics, Krakow, 1995), p. 196.
[27] D. Lupascu (unpublished).
[28] S. Hoth, Ph.D. thesis, University of Erlangen-Nürnberg, 1982.
[29] M. Iwatschenko-Borho, W. Engel, H. Foettinger, D. Forkel, F. Meyer, and W. Witthuhn, Nucl. Instrum. Methods Phys. Res. Sect. B **7/8**, 128 (1985).
[30] M. Uhrmacher, K. Pampus, F.J. Bergmeister, D. Purschke, and K.P. Lieb, Nucl. Instrum. Methods. Phys. Res. Sect. B **9**, 234 (1985).
[31] M. Neubauer, Ph.D. thesis, Universität Göttingen, 1993.
[32] D. Wieshow and H. Ruppert (private communication).
[33] D.J.M. Bevan and E. Summerville, in *Handbook on the Physics and Chemistry of the Rare Earths*, edited by K.A. Gschneidner, Jr. and L. Eyring (North-Holland, Amsterdam, 1979), p. 401.
[34] G. Rienäcker and Y. Wu, Z. Anorg. Chem. **315**, 121 (1962).
[35] A. Rabeneau, Z. Anorg. Allg. Chem. **288**, 221 (1956).
[36] R.T. Cox, Solid State Commun. **9**, 1989 (1971).
[37] J. Rudolph, Z. Naturforsch. **14a**, 727 (1959).
[38] G.V. Subba Rao, S. Ramdas, P.N. Mehrotra, and C.N.R. Rao, J. Solid State Chem. **2**, 377 (1970).
[39] Y. Wilbert, N. Dherbomez, and H. Breuil, C.R. Acad. Sci. Ser. C **280**, 373 (1975); **280**, 465 (1975).
[40] T. Norby, O. Dyrlie, and P. Kofstad, Solid State Ionics **53-56**, 446 (1992).
[41] W.D. Schneider, B. Delley, E. Wuilloud, J. M. Imer, and Y. Baer, Phys. Rev. B **32**, 6819 (1985).
[42] S. Hüfner, in *Handbook on the Physics and Chemistry of Rare Earths*, edited by K.A. Gschneider, Jr., L. Eyring, and S. Hüfner (North-Holland, Amsterdam, 1987), Vol. 10, p. 301.
[43] W. Noddak and H. Walch, Z. Elektrochem. **63**, 269 (1959).
[44] Y. Imry and Z. Ovadyahu, Phys. Rev. Lett. **49**, 841 (1982).
[45] I. Schwarz, S. Shaft, A. Moalem, and Z. Ovadyahu, Philos. Mag. B **50**, 221 (1984).
[46] T. Takizawa, C. Komatsu, H. Matsushita, A. Goltzené, and C. Schwab, J. Cryst. Res. Technol. (to be published).
[47] A. Miller and E. Abraham, Phys. Rev. **120**, 145 (1960).
[48] M. Lannoo and J. Bourgoin, *Point Defects in Solids* (Springer, Berlin, 1981).
[49] B.H. Justice and E.F. Westrum, Jr., J. Phys. Chem. **67**, 339 (1963).

[50] D. Wiarda, M. Uhrmacher, A. Bartos, and K.P. Lieb, J. Phys. Condens. Matter **5**, 4111 (1993).
[51] R.N. Attili, M. Uhrmacher, K.P. Lieb, L. Ziegeler, M. Mekata, and E. Schwarzmann, Phys. Rev. B **53**, 600 (1996).
[52] M.C. Mahapatra, P.C. Pattnaick, M.D. Thomson, and T.P. Das, Phys. Rev. B **16**, 3001 (1977).
[53] P. Aldebert and J.P. Traverse, Mater. Res. Bull. **14**, 303 (1979).
[54] X. Oudet, Ann. Chim. Phys. **8**, 483 (1983); J. Magn. Magn. Mater. **47&48**, 397 (1985).
[55] Th. Wichert, N. Achtziger, H. Metzner, and R. Sielemann, in *Hyperfine Interactions of Defects in Semiconductors*, edited by G. Langouche (Elsevier Science, Amsterdam, 1992), p. 96 ff.
[56] *CRC Handbook of Chemistry and Physics 60*, edited by R. Weast and M.J. Astle (CRC Press, Boca Raton, 1979).